Phys Chem Minerals (2003) 30: 108 – 124
DOI 10.1007/s00269-002-0291-1

ORIGINAL PAPER

J. Najorka · M. Gottschalk

Crystal chemistry of tremolite–tschermakite solid solutions

Received: 9 November 2002 / Accepted: 11 November 2002

Abstract Tremolite–tschermakite solid solutions have been synthesized between 700 and 850 °C and 200 and 2000 MPa. The starting materials were oxide–hydroxide mixtures and an additional 0.1–1.8 molal $CaBr_2$ solution. The run products were characterized using SEM, HRTEM, EMP, XRD and FTIR. The synthesized Al tremolites formed needles and lath-shaped crystals of up to 300 × 20 μm. HRTEM investigations showed that the majority of the amphiboles were well ordered. The EMP analysis revealed that the Al tremolites were solid solutions in the ternary tremolite–tschermakite–cummingtonite. The highest observed Al content was close to the composition of magnesiohornblende ($X_{ts} = 0.54$). Different cummingtonite concentrations ($X_{cum} = 0.00$–0.18) were observed, which generally increased with Al content. Rietveld refinements of the lattice constants showed a linear decrease of the cell parameters a and b with increasing Al content, whereas c and β increased. Small deviations from the linear behaviour were caused by variable amounts of the cummingtonite component. For pure tschermakite lattice parameters of $a = 9.7438(11)$ Å, $b = 17.936(14)$ Å, $c = 5.2995(3)$ Å, $\beta = 105.68(9)°$ and $V = 891.7 \pm 1.4$ Å^3 were extrapolated by least-squares regression. Using the a and β lattice parameters for tremolite, tschermakite and cummingtonite, it was possible to derive amphibole compositions using powder XRD. IR spectra of the Al tremolites showed a total of 12 individual bands. The FWHMs of all bands increased with increasing Al content. According to their FWHMs, these bands were grouped into three band systems at 3664–3676 cm^{-1} (I), 3633–3664 cm^{-1} (II) and 3526–3633 cm^{-1} (III). Assuming $^{[6]}$Al substitution at M2 and/or M3 and $^{[4]}$Al at T1, three principal different configurational groups could be assigned as local environments for the proton. I: only Si^{4+} at T1 and one or two Al^{3+} at M2 and/or $M3_{far}$, II: one Al^{3+} at T1 and one to three Al^{3+} at M2 and/or at $M3_{far}$, III: either Al^{3+} on $M3_{near}$ and/or two Al^{3+} on T1 and additional one to four Al^{3+} at M2. It is assumed that these three configurational groups correspond to the three groups of observed bands. This was quantitativly supported by Monte-Carlo simulations. A model with random distribution at M2 and M3 including Al avoidance at tetrahedral and octahedral sites yielded the best agreement with the spectroscopical results.

Keywords Amphibole · Tremolite · Tschermakite · Rietveld refinement · IR spectroscopy

M. Gottschalk · J. Najorka (✉)
GeoForschungszentrumPotsdam
Telegrafenberg
14473 Potsdam
Germany
e-mail: gottschalk@gfz-potsdam.de
Tel.: +49-(0)331-288-1418
Fax: +49-(0)331-288-1402

Present address: J. Najorka
Corus Research, Development & Technology
Ceramics Research Centre
Wenckebachstraat 1
1951 JZ Velsen-Noord
The Netherlands
e-mail: Jens.Najorka@corusgroup.com
Tel.: +31 2514 93831
Fax: +31 2514 70489

Introduction

In rock-forming silicates such as amphiboles, pyroxenes, micas and chlorites, the Mg tschermakite substitution of the type $Mg^{2+} + Si^{4+} = Al^{3+} + Al^{3+}$ is quite common. Generally, the amount of the tschermakite component is controlled by pressure, temperature and bulk composition or is even buffered by a phase assemblage. In the latter case, if the thermodynamic properties of this substitution were understood, the Al content could be used for geothermobarometric purposes.

The content of the tschermakite component in amphiboles has been studied experimentally by Jasmund and Schäfer (1972), Oba (1978), Cao et al. (1986),

Jenkins (1981, 1983, 1988, 1994) Jenkins et al. (1997), Cho and Ernst (1991), Smelik et al. (1994), Hoschek (1995), Quirion and Jenkins (1998) and Hawthorne et al. (2000) using the simplified system tremolite–aluminotschermakite, $Ca_2Mg_5[Si_8O_{22}/(OH)_2]$–$Ca_2Mg_3Al_2$ [$Al_2Si_6O_{22}/(OH)_2$], a system hereafter referred to as tremolite–tschermakite. The synthetic tremolite-tschermakite crystals were usually very small and the fibrous needles rarely exceeded a thickness of 5 μm. The small grain size made chemical characterization using the electron microprobe difficult if not impossible. To avoid preparation difficulties, unpolished grain mounts were often used for EMP analyses (Cao et al. 1986; Jenkins 1988, 1994; Hoschek 1995; Quirion and Jenkins 1998). The precision of this method is rather low and standard deviations are on the order of 5% (Jenkins 1994). Several investigations (Jenkins 1981, 1983, 1988, 1994; Cho and Ernst 1991; Hoschek 1995) used the *d*-value variation of the (310) reflection as a function of composition for the determination of the Al content in tremolite-tschermakite solid solutions. The uncertainty when using this approach is also high, however (6%, Cho and Ernst 1991), and the influence of additional components (e.g., cummingtonite) is generally neglected. Therefore, the analytical error in the chemical composition of most of the previously synthesized tremolite–tschermakite solid solutions seems to be large.

In addition to uncertainties in composition, the crystal chemistry of Al^{3+} in tremolite–tschermakite solid solutions has not been resolved univocally. A fragment of the structure of the monoclinic *C* 2/*m* amphiboles is shown in Fig. 1. The main feature of the amphibole structure is two double chains of SiO_4 tetrahedra connected by a strip of octahedra which form an *I* beam in the *z* direction. In tremolite the octahedra sites M1, M2 and M3 are occupied by Mg^{2+}, M4 by Ca^{2+} and the tetrahedra sites T1 and T2 by Si^{4+}.

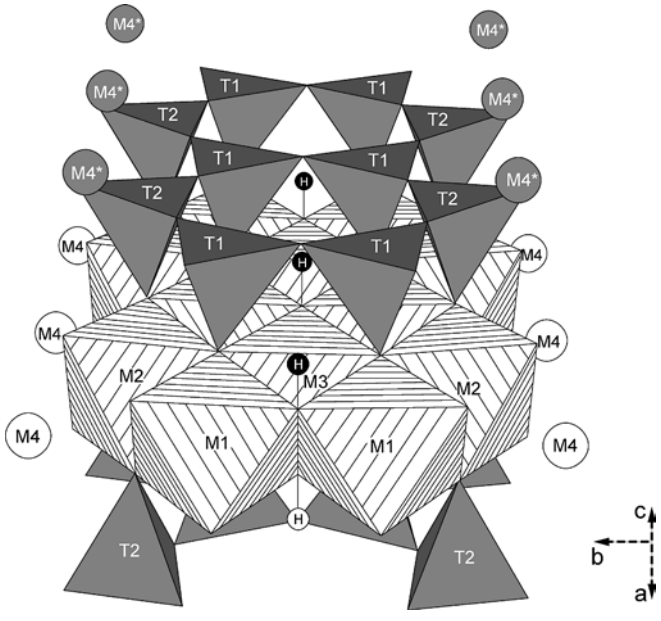

Fig. 1 *I* beam of the *C* 2/*m* amphibole structure with surrounding M4 sites. A strip of edge-sharing octahedra is intercalated between two corner-sharing double tetrahedral chains in apex-to-apex arrangement. The M2 and M4 sites provide the linkages to adjacent *I* beams. (After Hawthorne 1983)

Using natural monoclinic amphibole, Hawthorne (1981) deduced from mean bond length vs. ionic radius relationships that octahedral Al^{3+} ($^{[6]}Al$) is strongly ordered on the M2 site. IR and NMR studies of synthetic pargasites indicated $^{[6]}Al$ disorder over M2, M1 and/or M3 sites (Raudsepp et al. 1987; Welch 1994). Single-crystal X-ray structure refinements of natural pargasites and pargasitic hornblendes (Oberti et al. 1995a) showed that octahedral Al^{3+} is distributed over the M2 and M3 sites. This is in accordance with a neutron powder diffraction study of synthetic pargasite (Welch and Knight 1999) and an IR investigation of synthetic richterite–pargasite solid solutions (Della Ventura et al. 1999). In a recent study, synthetic tremolite–magnesiohornblende solid solutions were investigated by Hawthorne et al. (2000) using IR and NMR techniques. The spectra indicated that $^{[6]}Al$ occupies two different octahedral sites, the M2 site and the M1 or M3 site.

In monoclinic amphiboles tetrahedral Al ($^{[4]}Al$) is preferentially incorporated on the T1 site (Hawthorne 1981) which was derived from mean bond-length considerations. Oberti et al. (1995b) showed in a single-crystal study of calcic amphiboles that for amphiboles with contents of $^{[4]}Al < 2$ atoms per formula unit (apfu), Al^{3+} strongly prefers the T1 site. However, Al^{3+} on T1 and T2 sites is observed in amphiboles with $^{[4]}Al > 2$ apfu. Al^{3+} disorder over T1 and T2 sites is also a function of temperature (Oberti et al. 1995b). This is in agreement with ^{29}Si MAS NMR investigations (Welch et al. 1998) of pargasite synthesized at 930 °C and 100 MPa. Al^{3+} ordering on the T1 site was observed, however, in fluoro-edenite synthesized at 1000 °C and 200 MPa (Welch et al. 1998).

Jenkins et al. (1997) investigated synthetic tremolite–tschermakite solid solutions up to the composition of magnesiohornblende, $Ca_2Mg_4Al[AlSi_7O_{22}/(OH)_2]$, using EMP, XRD, IR and NMR. This study indicated that Al^{3+} is distributed over all T and M sites in the Al tremolites. However, a detailed quantitative analysis of the site occupancies for Al^{3+} was not possible.

Difficulties in the determination of site occupancies of Al^{3+} in synthetic Al tremolites are due mainly to the following reasons. Similar X-ray scattering factors for Al, Si and Mg make site-scattering refinements using XRD data very difficult, if not impossible. In addition, due to the small grain size of the synthetic tremolite–tschermakite solid solutions, single-crystal X-ray diffraction studies of the site occupancies are not possible; and finally, the band broadening of the IR and NMR spectra in Al-rich tremolite makes the quantitative interpretation of Al^{3+} occupancies difficult (Jenkins et al. 1997; Hawthorne et al. 2000).

The derivation of thermodynamic mixing properties, however, requires a knowledge of the crystal chemistry, especially if these are to be applied over a larger P–T range than obtained experimentally. Entropies of ideal mixing are crucial for the derivation of such models. Therefore, if the amount of tschermakite substitution is to be used as a petrogenetic indicator, a good knowledge of the site occupancies for $^{[4]}$Al and $^{[6]}$Al along the tremolite–tschermakite join is needed.

In this study, amphiboles along the tremolite-tschermakite join were synthesized in the presence of halogenidic fluids. With this method it was possible to obtain amphibole crystals that were large enough for electron microprobe measurements (cf. Zimmermann et al. 1996; Gottschalk et al. 1998; Melzer et al. 1998). The synthesized tremolite–tschermakite solid solutions were characterized using scanning electron microscopy (SEM), high-resolution transmission electron microscopy (HRTEM), electron microprobe (EMP), powder X-ray diffraction (XRD) and Fourier transform infrared spectroscopy (FTIR). The combination of results from EMP and XRD were used for the derivation of a more precise method to deduce the compositions of the amphiboles from lattice parameters in the ternary system tremolite–tschermakite–cummingtonite. Quantitative $^{[6]}$Al site occupancies were derived using IR spectroscopy of the OH-stretching vibration in conjunction with derived compositions of the tremolite–tschermakite solid solutions.

Experimental and analytical techniques

Experimental methods

The experiments were performed using standard cold-seal hydrothermal and piston-cylinder techniques. The hydrothermal experiments were carried out between 700 and 800 °C and 200 and 500 MPa using H_2O and CO_2 as a pressure medium. Temperatures were measured close to the sample with an Ni–CrNi thermocouple, and were accurate within ± 5 °C, pressures were measured with a calibrated strain gauge with a precision of ± 5 MPa. At the end of each run, the samples were quenched isobarically with compressed air to 300 °C within 3 min.

The piston cylinder experiments were performed between 700 and 850 °C and 1150 and 2000 MPa. The accuracy of the temperature measurement with the Ni–CrNi thermocouple was ± 15 °C. The pressure uncertainties were ± 50 MPa. NaCl (T < 800 °C) and CaF_2 (T > 800 °C) assemblies were used. Because of its higher friction for the CaF_2 assemblies, the pressure had to be corrected by 10%.

Mixtures of SiO_2, MgO, Al_2O_3 and $Ca(OH)_2$ (analytical grade) and a 0.1–1.8 molal aqueous $CaBr_2$ solution were used as starting materials. The solid/fluid ratio varied between 0.5 and 3.0. The bulk compositions of the runs were chosen to be close to but not on the tremolite–tschermakite join. An excess of SiO_2 (3–8 wt%) was used in order to compensate for the solubility of SiO_2 at P and T (Manning 1994). The samples for the hydrothermal experiments were sealed in gold capsules of 25–35 × 3 mm with a wall thickness of 0.2 mm. For the piston-cylinder runs, platinum and gold capsules of 10–12 × 3 mm and a wall thickness of 0.2 mm were used. The charges contained between 30 and 60 mg solids and 30 and 60 mg fluid in the hydrothermal runs and between 6 and 12 mg solids and 2 and 6 mg fluid in the piston-cylinder runs. The run charges and the synthesis conditions of the experiments are listed in Table 1.

Table 1 Run charges and synthesis conditions

Run	$Ca(OH)_2$ (mg)	$CaBr_2$ (mg)	MgO (mg)	Al_2O_3 (mg)	SiO_2 (mg)	H_2O (mg)	$CaBr_2$-molality	T (°C)	P (MPa)	Time (days)
TS-6	4.04	1.31	5.22	1.05	14.98	50.91	0.13	750	500	26
TS-15	3.56	5.71	4.61	0.61	11.98	28.56	0.97	750	500	7
TS-16	3.55	5.71	2.91	4.89	9.40	28.55	0.97	750	500	7
TS-18	1.48	1.70	1.47	1.09	4.62	8.49	0.96	800	1500	5
TS-19	1.43	1.70	1.59	0.88	4.74	8.52	0.96	800	1500	5
TS-20	3.70	2.85	4.35	0.75	11.65	14.28	0.94	800	200	7
TS-30	5.15	5.73	5.86	4.11	15.39	28.66	0.96	750	500	14
TS-33	5.59	5.71	6.59	0.89	17.34	28.55	0.95	750	500	30
TS-40	4.68	3.52	5.20	1.34	14.51	17.58	0.94	750	350	17
TS-41	4.69	6.84	5.38	0.97	14.56	34.21	0.97	700	350	27
TS-48	1.54	2.12	1.35	1.09	4.78	10.58	0.97	750	1500	7
TS-50	1.54	2.30	1.36	1.08	5.00	11.53	0.97	750	2000	7
TS-52	1.07	0.97	1.26	0.98	5.25	10.14	0.47	850	1500	5
TS-53	1.05	0.97	1.27	0.97	5.64	10.17	0.47	850	2000	10
TS-54	1.13	1.01	1.28	0.76	4.76	9.92	0.50	800	1500	13
TS-56	2.62	2.35	3.77	1.19	10.73	30.07	0.38	750	350	14
TS-64	4.17	3.75	5.41	1.61	15.74	45.70	0.40	750	200	14
TS-70	1.57	1.49	1.24	1.21	4.95	4.96	1.40	750	1500	7
TS-82	6.82	6.16	9.45	4.22	23.69	25.06	1.15	800	200	14
TS-83	5.85	5.31	11.14	0.56	27.64	25.06	1.00	800	200	14
TS-86	8.19	7.37	12.72	3.91	27.84	19.88	1.69	800	200	14
TS-90	1.48	1.37	2.14	1.35	6.55	5.98	1.08	850	1150	6
TS-91	1.73	1.54	1.56	1.59	6.48	5.97	1.21	850	1150	6
TS-92	1.92	0.92	1.65	2.35	5.55	2.45	1.58	850	1300	8
TS-93	1.69	0.94	2.21	1.40	6.13	2.58	1.57	850	1300	8
STR080	15.12[a]	10.07	14.21	10.27	40.34	28.65	1.76	700	500	14
TR-II-5[b]	43.43[a]	–	114.15	–	272.38	80.00	0.00	660	700	50

[a] $CaCO_3$ instead of $Ca(OH)_2$
[b] Run TR-II-5 from Gottschalk et al. (1999)

Analytical methods

The synthesized products were characterized by optical, scanning electron (SEM) and high-resolution transmission electron microscopy (HRTEM), electron microprobe (EMP), powder X-ray diffraction (XRD) and Fourier transform infrared spectroscopy (FTIR).

The SEM and HRTEM investigations were performed using a Zeiss DSM962 scanning electron microscope and a Philips CM200T transmission electron microscope. The EMP analyses were performed on polished and carbon coated samples with Cameca SX50 and SX100 microprobes. The data were collected in wavelength dispersive spectrometry mode and corrected using the PAP program (Pouchou and Pichoir 1984). The following standards were used: wollastonite for Si and Ca, synthetic plagioclase for Al and natural tremolite for Mg. Peak counting times were 40 s for Ca and Mg and 20 s for Si and Al. For the background, counting times were 20 and 10 s, respectively.

For XRD measurements, the solid-run products were ground in an agate mortar to a grain size of less than 2 μm. The powder was diluted with Elmer's White glue and mounted on a circular foil. To minimize preferred orientation, the powder was stirred during drying. The foil was then placed into the sample holder and covered with a second empty foil. Powder XRD patterns were recorded in transmission using a fully automated STOE STADI P diffractometer (Cu $K_{\alpha 1}$ radiation), equipped with a primary monochromator and a 7°-wide position sensitive detector (PSD). Operating conditions were 40 kV and 40 mA, with a takeoff angle of 6°. The spectra were recorded in the range of 5 to 125° (2θ) using a step interval of 0.1°. The resolution of the PSD was set to 0.02°. Counting times were selected to yield a maximum intensity of 2000 to 3000 counts for each sample, resulting in 5 to 20 s per detector step. The unit-cell and other structural parameters were refined using the GSAS software package for Rietveld refinement (Larson and Von Dreele 1987). The isotropic displacement factors of tremolite were fixed at values approximately correct for amphiboles (Della Ventura et al. 1993). The following algorithm was used during the refinement procedure: scale factor, background (real space correlation function), zero-point correction, phase fractions, lattice constants, Caglioti W, preferred orientation, atomic positions, Caglioti U + V, and Lorentz LX + LY. Further details of the refinement procedure are described by Gottschalk and Andrut (1998).

IR absorption spectra were recorded in the spectral range of 3500 to 3800 cm^{-1} with a resolution of 0.25 cm^{-1} using a Bruker IFS 66V FTIR spectrometer equipped with a globar light source, a KBr beam splitter and a DTGS detector. The sample chamber was evacuated to 300 Pa. Transparent pellets (mixtures of 1 mg amphibole and 450 mg KBr) were pressed under vacuum and dried at 170 °C for at least 48 h, but typically for several weeks. The spectra were averaged over 1024 scans and evaluated using the program PeakFit (SPSS Science). The background was subtracted using in most cases a linear function and only in some cases a cubic function. A combination of a Gaussian and a Lorentzian function with equal full width at half maximum (FWHM) was used to fit the bands.

Results

REM

Typical SEM images of the synthesized products are shown in Fig. 2. Amphibole was the principal phase in the experiments and formed idiomorphic needle or lath-shaped crystals with widths of 1–20 μm and lengths of 10–300 μm. In general, the grain size of the amphiboles increased with rising P–T conditions as well as with increasing concentration of the bromidic solution. The thinnest amphibole needles were synthesized at 200–500 MPa and 750 °C, where the grain width rarely exceeded 3 μm (Fig. 2c). At 800 °C and 200 MPa, many crystals with a thickness of 5–10 μm were observed (Fig. 2d). High pressures runs between 1.3 and 2.0 GPa generally yielded large amounts of amphiboles with lath-shaped habitus and a thickness of up to 10–20 μm (Fig. 2a, b). Amorphous SiO_2 was observed in several runs (e.g., Fig. 2b).

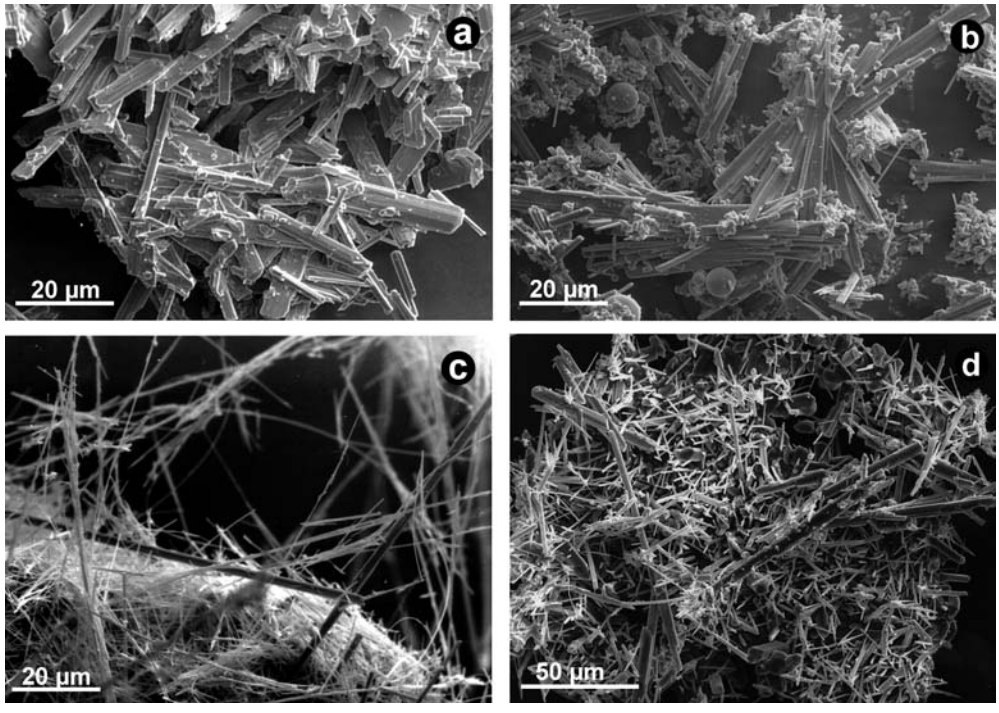

Fig. 2a–d Typical SEM images of the synthesized amphiboles from high pressure runs (≥1150 MPa) (**a, b**) and low pressure runs (≤500 MPa) in (**c, d**). Lath-shaped amphiboles with **a** $X_{ts} = 0.54$ (run TS-93) and **b** $X_{ts} = 0.31$ (run TS-70). **c** Amphibole needles from run TS-6 ($X_{ts} = 0.22$). **d** Needle to lath-shaped amphiboles from run TS-20 ($X_{ts} = 0.12$)

HRTEM

Al tremolites from runs TS-6, TS-15, TS-16, TS-18, TS-19, TS-20, TS-33, TS-41, TS-52, TS-64, and TS-93 were investigated by HRTEM. Figure 3a, b shows representative HRTEM images of the synthesized amphiboles. The majority of the Al tremolites were well ordered with only a minor concentration of chain multiplicity faults (≤5%). Higher concentrations of chain multiplicity faults (≈10%) were observed only in runs TS-15 and TS-33 (Fig. 3b). Figure 3b shows an Al tremolite crystal of run TS-33 with 40 double-chain units, 3 triple- and 2 quadruple-chain multiplicity faults. Typically single-, triple-, quadruple- and quintuple-chain multiplicities faults were observed. Faults with multiplicities ≥3 occurred mostly as isolated chains and passed through the whole crystal. High overall chain fault concentrations were often observed to be concentrated in small areas of the crystal.

EMP

Except for the runs TS-6, TS-15, TS-30, TS-40 and TS-83, the compositions of the synthesized amphiboles were determined by EMP. These results are presented in Table 2. The analyses were normalized to 23 oxygens, and the cations were distributed according to the formula $AB_2C_5[T_8O_{22}/(OH)_2]$ (A = vacant; B = Ca, Mg; C = Mg, Al; T = Al, Si). The total Al content was distributed equally ($Al^{tot}/2$) over the C and T sites, assuming that tschermakite substitution is obeyed. A single analysis was accepted if the total oxide sum was in the range of 91–99 wt%. Because of the small crystal size of the amphiboles in run TS-64, the total oxide sum were mostly below 90 wt%. Therefore, a total oxide sum between 85 and 99 wt% was accepted for amphiboles from run TS-64. Some analyses showed unusually high T-site occupancies larger than 8. From a crystal-chemical view, such occupancies are not allowed, and are believed to be an analytical artefact. Therefore site occupancies were used as additional criteria if these deviations were larger than the analytical error (2σ). If the site occupancies exceeded the nominal value by ±1% on the T sites, ±2% on the B and C sites and ±0.5% for the total sum of all cation sites (=15) the analysis was also rejected.

The average amphibole compositions of the runs are summarized in Table 2 and Fig. 4. The synthesized Al tremolites are solid solutions of the ternary tremolite–tschermakite–cummingtonite. Along the tschermaks vector $Si_{-1}Mg_{-1}Al_2$, amphibole compositions were between 11 and 54 mol% tschermakite. The Al-richest composition was observed in run TS-93 ($X_{ts} = 0.54$), which is close to the composition of magnesiohornblende. Ca^{2+} was replaced, to a small extent, by Mg^{2+} on the M4 site and cummingtonite concentrations of up to $X_{cum} = 0.18$ were observed. The cummingtonite content for most runs was in the range of $X_{cum} = 0.00$–0.10, however. Br contents were always below the detection limit (< 0.1 wt%).

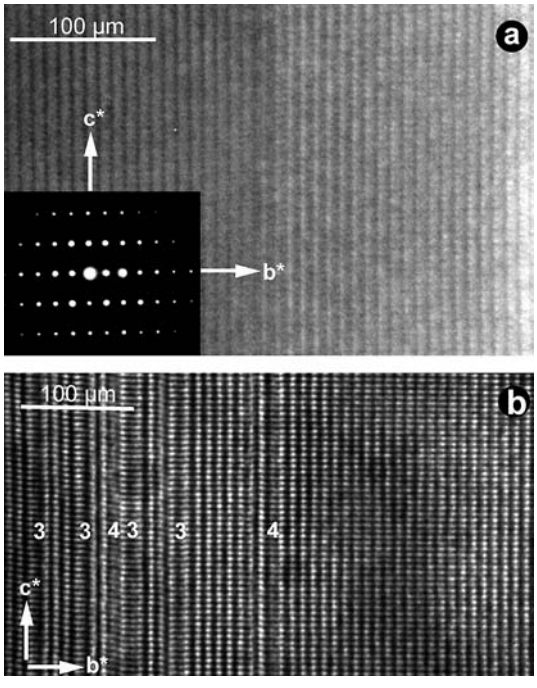

Fig. 3a, b HRTEM images of (020) lattice fringes of the synthesized amphiboles. **a** A defect-free amphibole crystal from run TS-19 ($X_{ts} = 0.32$). **b** Randomly distributed triple and quadruple chains in an amphibole crystal from run TS-33 ($X_{ts} = 0.13$)

XRD

A Rietveld structure refinement was performed for each run product. The derived phase proportions and amphibole lattice parameters are presented in Table 3. The amphibole yield was between 40 and 100 wt%. Up to three additional minor solid phases were detected. These were quartz, anorthite, diopside, talc, chlorite, zoisite and enstatite.

Figure 5 shows that the lattice parameters of the synthesized amphiboles are a linear function of the Al content. With increasing amount of Al substitution in tremolite, the cell parameters a and b decrease whereas the parameters c and β increase. Some variations are observed for the lattice parameters a and β. These variations correlate with the amount of cummingtonite component in Al tremolite (see below). As a result of increasing cummingtonite content, the values of the a and β parameters decrease.

IR

Powder spectra were recorded in the range of OH-stretching vibrations between 3500 and 3800 cm^{-1} and are shown in Fig. 6. Only samples with > 70 wt%

Table 2 Composition of the synthesized Al tremolites

Run	TS-16	TS-18	TS-19	TS-20	TS-33	TS-41	TS-48	TS-50	TS-52	TS-53	TS-54	TS-56	TS-64	TS-70	TS-82	TS-86	TS-90	TS-91	TS-92	TS-93	STR080
No. of analyses	15	10	3	20	2	3	8	14	23	20	32	7	8	18	12	8	13	9	26	35	23
CaO	12.40	12.21	11.84	13.05	13.27	13.50	13.02	12.97	11.25	13.01	12.85	12.23	11.98	12.76	12.33	12.15	11.85	12.96	12.15	12.20	13.16
MgO	20.63	21.35	21.04	23.22	23.89	22.76	22.24	22.77	22.83	22.69	21.78	23.18	21.79	22.52	24.05	23.69	22.42	21.54	21.07	20.05	21.17
Al_2O_3	10.20	8.33	8.00	2.83	2.76	3.07	6.82	4.91	8.85	6.91	7.81	6.78	3.49	7.79	3.30	4.27	7.96	8.84	11.21	13.36	9.19
SiO_2	51.23	52.52	50.56	56.46	57.60	56.58	54.33	55.68	53.50	54.94	54.35	55.78	51.31	54.93	56.83	56.10	54.37	54.70	52.84	50.81	53.65
Σ oxides	94.45	94.42	91.44	95.56	97.52	95.90	96.41	96.33	96.42	97.54	96.78	97.97	88.56	98.01	96.50	96.21	96.59	98.03	97.27	96.43	97.18
2σ standard deviation of the mean																					
ΔCaO	1.27	0.40	0.79	0.49	0.70	0.97	0.51	0.55	1.58	0.95	0.43	0.53	0.55	0.40	1.06	1.19	0.31	0.22	0.43	1.26	0.41
ΔMgO	2.41	2.11	0.48	1.42	0.54	0.86	1.54	1.33	2.26	1.06	1.29	0.88	1.39	1.06	1.82	1.17	0.85	1.10	1.31	1.20	1.20
ΔAl_2O_3	3.77	2.03	1.22	0.87	0.24	0.22	2.14	1.34	2.52	3.85	2.89	2.22	0.49	2.15	1.14	0.60	1.97	2.28	2.93	3.88	2.86
ΔSiO_2	3.38	2.70	1.25	2.70	0.80	1.47	3.51	2.66	2.93	1.65	1.63	1.46	3.63	1.88	3.12	3.18	1.81	1.60	1.72	3.17	2.34
Amphibole composition based on 23 oxygens																					
Ca	1.86	1.83	1.83	1.93	1.92	1.99	1.91	1.90	1.64	1.89	1.88	1.76	1.92	1.84	1.80	1.78	1.73	1.87	1.76	1.79	1.92
Mg	4.30	4.44	4.53	4.78	4.82	4.67	4.54	4.65	4.64	4.58	4.43	4.64	4.85	4.52	4.89	4.83	4.55	4.32	4.25	4.09	4.29
Al	1.68	1.37	1.36	0.46	0.44	0.50	1.10	0.79	1.42	1.10	1.25	1.07	0.62	1.23	0.53	0.69	1.28	1.40	1.79	2.15	1.47
Si	7.16	7.33	7.30	7.80	7.80	7.79	7.45	7.63	7.29	7.44	7.41	7.49	7.66	7.39	7.76	7.68	7.40	7.36	7.15	6.95	7.29
X_{ts}[a]	0.42	0.34	0.34	0.12	0.11	0.12	0.28	0.20	0.36	0.28	0.31	0.27	0.15	0.31	0.13	0.17	0.32	0.35	0.45	0.54	0.37
ΔX_{ts}[b]	0.07	0.04	0.02	0.02	0.00	0.01	0.05	0.03	0.05	0.08	0.06	0.04	0.01	0.04	0.02	0.02	0.04	0.05	0.06	0.07	0.05
X_{cum}[b]	0.07	0.09	0.08	0.03	0.04	0.00	0.04	0.05	0.18	0.06	0.06	0.12	0.04	0.08	0.10	0.11	0.14	0.07	0.12	0.11	0.03
X_{tr}	0.51	0.57	0.58	0.85	0.85	0.87	0.68	0.75	0.47	0.67	0.62	0.61	0.80	0.61	0.77	0.72	0.55	0.58	0.43	0.36	0.60
Σ M4	2.00	2.00	2.00	2.00	2.00	2.00	2.00	2.00	2.00	2.00	2.00	2.00	2.00	2.00	2.00	2.00	2.00	2.00	2.00	2.00	2.00
Σ M1-3[c]	5.00	4.96	5.04	4.94	4.96	4.91	5.01	4.95	4.99	5.02	4.93	4.94	5.07	4.98	4.96	4.96	4.92	4.89	4.91	4.95	4.94
Σ T[d]	8.00	8.02	7.98	8.03	8.02	8.04	8.00	8.02	8.00	7.99	8.04	8.03	7.96	8.01	8.02	8.02	8.04	8.06	8.05	8.02	8.03
Σ cations	15.00	14.98	15.02	14.97	14.98	14.96	15.00	14.98	15.00	15.01	14.96	14.97	15.04	14.99	14.98	14.98	14.96	14.94	14.95	14.98	14.97

[a] $X_{ts} = Al/4$
[b] $X_{cum} = (2 - Ca)/2$
[c] $\Sigma M1\text{-}3 = Mg - (2 - Ca) + Al/2$
[d] $\Sigma T = Al/2 + Si$

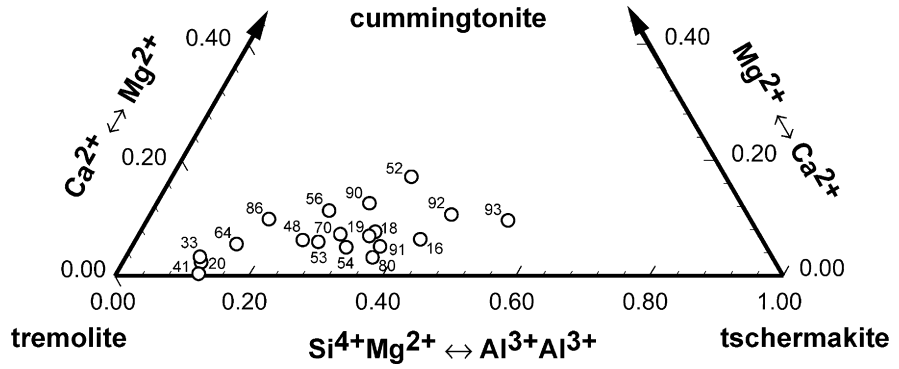

Fig. 4 Average compositions of the Al tremolites determined by EMP plotted in the ternary tremolite–tschermakite–cummingtonite. The Al-richest amphibole sample with $X_{ts} = 0.54$ (run TS-93) is close to the composition of magnesiohornblende. Variable cummingtonite contents are observed

amphibole and < 5 wt% of additional OH-bearing phases (chlorite, talc, zoisite) are shown. Starting from tremolite, systematic variations are observed with increasing Al content. A sharp band at 3675 cm^{-1} is visible in Al-poor tremolites. This band is known as the typical band of tremolite (e.g., Burns and Strens 1966). With increasing Al content in tremolite, the intensity of this band decreases, the band centre shifts to 3672 cm^{-1}, the full width at half maximum (FWHM) increases and additional bands centered at 3652, 3624 and 3608 cm^{-1} appears. With increasing Al content, the intensity and FWHM of these bands increase. Due to this broadening for Al-rich amphiboles ($X_{ts} > 0.30$) many bands overlapped.

Discussion

Phase composition and XRD

The EMP data show that the synthesized amphiboles are solid solutions in the ternary system tremolite–tschermakite–cummingtonite. A continuous solid solution series along the tremolite–tschermakite join up to roughly magnesiohornblende composition ($X_{ts} = 0.50$) with a maximum tschermakite content of $X_{ts} = 0.54$ was observed. Amphiboles with higher tschermakite contents could not be synthesized. This is in agreement with previous experimental studies (Cao et al. 1986; Jenkins 1988; Cho and Ernst 1991; Smelik et al. 1994; Hoschek 1995; Jenkins et al. 1997). Cho and Ernst (1991) synthesized amphiboles at 1250 MPa and 900 °C containing up to 60 mol% tschermakite. Oba (1978) has claimed to have synthesized pure tschermakite at 800–850 °C and 700–1700 MPa. However, this has never been reproduced (Jenkins 1988). Other syntheses with higher Al contents have not been reported yet. The crystal-chemical constraints for this limitation on the Al content is unknown. Only one eighth of all tetrahedral sites or only one quarter of the T1 sites are filled with Al^{3+} in magnesiohornblende and therefore Al avoidance seems not to be ultimatively involved. One may also speculate that the observed maximum Al content is not a rigid crystal chemical constraint but is due to systematic changes of the thermodynamic properties. Tremolite–tschermakite solid solutions could be simply less stable with respect to other assemblages containing phases like anorthite, corundum and melt. For otherwise fixed phase assemblages, the cummingtonite content of the amphibole (Gottschalk et al. 1999) increases with temperature. This seems also to be the case for the tschermakite content. In this case, before higher Al contents are reached, the amphibole decomposes to form a partial melt.

The measured cummingtonite concentrations were in the range of 0–18 mol%. At a constant tschermakite content, large variations in cummingtonite component were observed (Table 2; Fig. 4). In general, cummingtonite concentrations increased with increasing tschermakite content. As a consequence of the observed increasing cummingtonite content, phases like diopside, anorthite and zoisite become more abundant.

Cummingtonite as an additional component in synthetic tremolitic and richteritic amphiboles is widely observed (e.g., Jenkins 1987; Graham et al. 1989; Pawley et al. 1993; Smelik et al. 1994; Melzer et al. 2000) and concentrations of up to 10 mol% have been reported (Jenkins 1987). Because EMP analyses are often lacking, a cummingtonite content of 10 mol% had been assumed in synthetic Al tremolites (Jenkins 1994; Quirion and Jenkins 1998; Hawthorne et al. 2000).

The lattice parameters of the synthesized amphiboles are a systematic function of the Al content (Fig. 5) and cummingtonite concentration (Gottschalk et al. 1999). The a, b and β parameters of cummingtonite are significantly lower than those of tremolite. Therefore variations in lattice parameters (Fig. 5) are due to variations in cummingtonite content. It has been shown by Gottschalk et al. (1999) that for the system tremolite–cummingtonite the lattice parameters are a linear function of composition. Assuming that the lattice parameters are also a linear function of the Al content, and using the respective values for pure tremolite (Gottschalk et al. 1999) and cummingtonite (Hirschmann et al. 1994), the values $a = 9.7438(11)$ Å, $b = 17.936(14)$ Å, $c = 5.2995(3)$ Å, $\beta = 105.68(9)°$ and $V = 891.7 \pm 1.4$ $Å^3$ for tschermakite were obtained by least-squares regression and Eqs. (1)–(4) can be used to calculate the lattice parameters of tremolite–tschermakite–cummingtonite solid solutions.

Table 3 Results of the Rietveld refinement: statistics, phase proportions and lattice constants of the Al tremolites[a]

Run	R_p	R_{wp}	χ^2	DW	Phase proportions[b] (wt%)	a (Å)	b (Å)	c (Å)	β (°)	V (Å)	X_{ts}^{XRD}[d]	X_{ts}^{EMP}[e]
TS-6	0.073	0.054	1.63	1.27	90 amph + 9 di + 1 qtz	9.7860(10)	18.0282(13)	5.2801(3)	104.74(3)	900.9(1)	0.22	–
TS-15	0.057	0.042	1.48	1.32	90 amph + 7 di + 2 qtz + 1 tc	9.8033(2)	18.0356(12)	5.2781(3)	104.78(3)	902.3(1)	0.17	–
TS-16	0.075	0.057	1.63	1.19	40 amph + 24 an + 4 cln	9.7636(2)	17.9990(2)	5.2898(4)	104.90(1)	898.4(2)	0.42	0.42
TS-18	0.067	0.049	1.28	1.59	78 amph + 22 zo	9.7767(7)	18.0099(7)	5.2875(2)	104.84(2)	899.9(1)	0.33	0.34
TS-19	0.061	0.045	1.26	1.58	95 amph + 5 zo	9.7749(9)	18.0055(9)	5.2833(2)	104.82(2)	898.9(1)	0.32	0.34
TS-20	0.073	0.055	1.24	1.66	68 amph + 20 di + 6 qtz + 6 an	9.8138(4)	18.0516(5)	5.2798(1)	104.76(1)	904.5(1)	0.11	0.12
TS-30	0.061	0.045	1.60	1.25	76 amph + 24 an	9.7632(12)	18.0090(18)	5.2835(1)	104.74(1)	898.4(2)	0.32	–
TS-33	0.062	0.046	1.35	1.43	74 amph + 4 qtz	9.8083(8)	18.0434(14)	5.2766(3)	104.76(3)	903.0(1)	0.13	0.11
TS-40	0.063	0.046	1.86	1.20	66 amph + 18 di + 10 an + 6 qtz	9.8009(15)	18.0449(31)	5.2790(7)	104.80(7)	902.6(2)	0.19	–
TS-41	0.062	0.065	1.36	1.38	64 amph + 30 di + 6 qtz	9.8082(12)	18.0423(22)	5.2772(4)	104.80(4)	902.9(2)	0.16	0.12
TS-48	0.059	0.043	1.41	1.44	73 amph + 21 zo + 6 tc	9.7913(6)	18.0178(6)	5.2808(1)	104.86(1)	900.5(1)	0.27	0.28
TS-50	0.065	0.048	1.27	1.57	43 amph + 33 zo + 22 tc + 1 qtz	9.8034(8)	18.0323(10)	5.2817(2)	104.83(4)	902.6(1)	0.20	0.20
TS-52	0.064	0.047	1.34	1.48	99 amph + 1 zo	9.7516(7)	17.9890(8)	5.2836(2)	104.76(2)	896.3(1)	0.39	0.36
TS-53[c]	0.062	0.046	1.27	1.53	59 amph + 34 di + 7 fluorite	9.7913(11)	18.0048(9)	5.2813(2)	104.82(2)	900.1(1)	0.24	0.28
TS-54	0.080	0.058	1.31	1.49	91 amph + 9 zo	9.7850(7)	18.0126(6)	5.2835(1)	104.90(1)	899.9(1)	0.33	0.31
TS-56	0.072	0.054	1.42	1.41	74 amph + 11 qtz + 11 an + 4 tc	9.7790(8)	18.0276(17)	5.2805(4)	104.72(4)	900.4(1)	0.24	0.27
TS-64	0.078	0.059	1.43	1.37	67 amph + 24 an + 9 qtz	9.7976(7)	18.0371(13)	5.2787(3)	104.75(3)	902.1(1)	0.18	0.15
TS-70	0.047	0.035	1.37	1.41	63 amph + 29 zo + 6 qtz + 2 tc	9.7822(5)	18.0119(7)	5.2816(1)	104.84(1)	899.6(1)	0.30	0.31
TS-82	0.059	0.043	1.29	1.47	69 amph + 21 an + 8 en + 2 qtz	9.7874(5)	18.0373(7)	5.2777(2)	104.65(2)	901.4(1)	0.16	0.13
TS-83	0.069	0.051	1.26	1.57	80 amph + 13 qtz + 7 en	9.8024(5)	18.0450(6)	5.2767(2)	104.64(2)	903.0(1)	0.08	–
TS-86	0.068	0.050	1.36	1.52	70 amph + 18 en + 12 an	9.7949(4)	18.0391(5)	5.2800(1)	104.75(1)	902.2(1)	0.19	0.17
TS-90	0.058	0.042	1.27	1.55	97 amph + 2 en + 1 tc	9.7601(5)	18.0071(8)	5.2830(2)	104.75(2)	897.9(1)	0.34	0.32
TS-91	0.057	0.042	1.23	1.54	100 amph	9.7694(5)	18.0011(9)	5.2827(2)	104.87(2)	897.9(1)	0.37	0.35
TS-92	0.070	0.051	1.49	1.38	100 amph	9.7480(5)	17.9821(8)	5.2898(2)	104.83(2)	896.4(1)	0.44	0.45
TS-93	0.065	0.046	1.44	1.34	78 amph + 18 an + 4 cor	9.7457(8)	17.9610(11)	5.2903(3)	104.93(3)	894.8(1)	0.52	0.54
STRO80	0.063	0.047	1.47	1.36	69 amph + 24 an + 7 tc	9.7740(7)	17.9961(10)	5.2848(2)	104.87(2)	898.4(1)	0.36	0.37
TR-II-5	0.083	0.064	1.31	1.56	95 amph + 4 di + 1 qtz	9.8364(5)	18.0540(8)	5.2768(2)	104.73(2)	906.3(1)	0.00	0.00

[a] $R_p = \sum |y_i^{obs} - y_i^{calc}| / \sum y_i^{obs}$, $R_{wp} = \sqrt{\sum w_i (y_i^{obs} - y_i^{calc})^2 / \sum w_i (y_i^{obs})^2}$, $\chi^2 = \sum w_i (y_i^{obs} - y_i^{calc})/(N - P)$, y: intensity, w: $1/y$ weighting factor, N-P: observations (step intervals) – least-squares parameters; DW: Durbin-Watson statistics

[b] Amph amphibole, di diopside, qtz quartz, tc talc, zo zoisite, en enstatite, cor corundum

[c] Fluorite content in run TS-53 was caused by impurity induced from the pressure medium after experiment

[d] X_{ts}^{XRD} is tschermakite content derived from lattice constant

[e] X_{ts}^{EMP} is tschermakite content derived from microprobe analysis

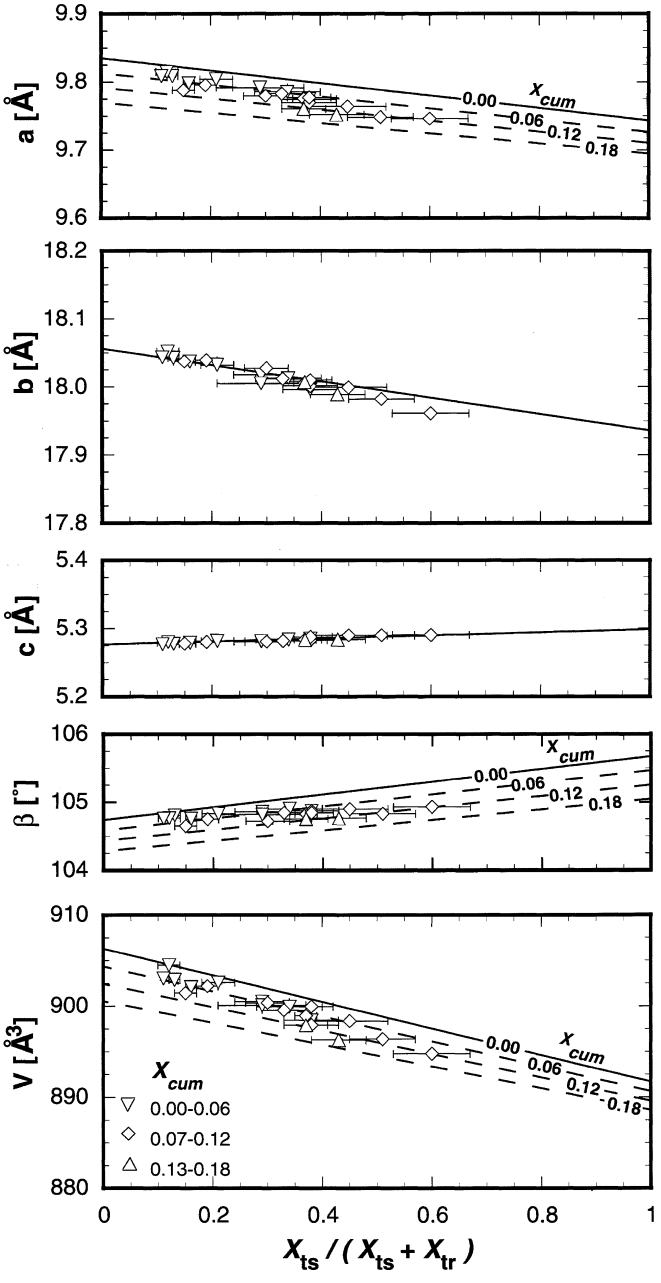

Fig. 5 Lattice constants a, b, c, β and cell volume V of the synthesized Al tremolites as a function of $X_{ts}/(X_{ts} + X_{tr})$ determined by EMP. Cummingtonite isopleths are as *solid lines* for $X_{cum} = 0.00$ and as *dashed lines* for $X_{cum} = 0.06$, 0.12 and 0.18. Cummingtonite isopleths were calculated from Eqs. (1)–(4)

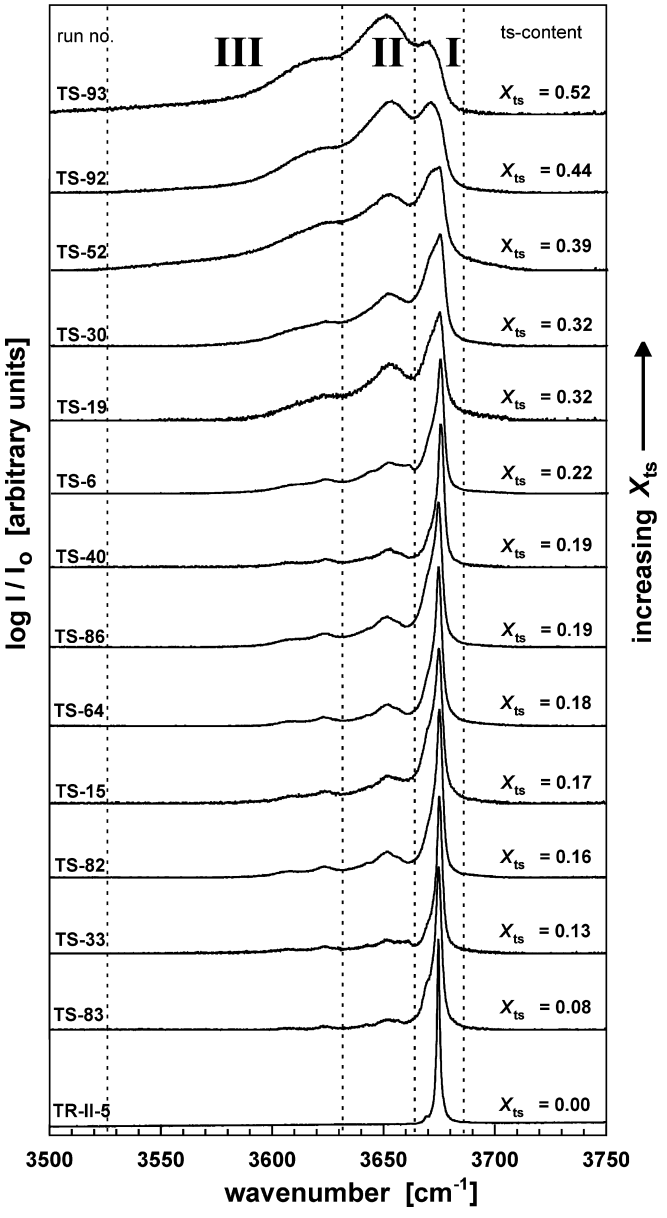

Fig. 6 FTIR spectra of the OH-stretching vibration of Al tremolites (background subtracted). The spectra are sorted with increasing values of X_{ts}, derived from XRD data. The sharp band in Al-poor tremolites at 3675 cm^{-1} decreases with increasing X_{ts} and new bands appear at 3652, 3624 and 3608 cm^{-1}. The FWHMs of all bands increase with increasing X_{ts}. Three band regions were distinguished at 3664–3676 cm^{-1} (*I*), 3633–3664 cm^{-1} (*II*) and 3526–3633 cm^{-1} (*III*) (see text)

$$a[\text{Å}] = 9.8354X_{tr} + 9.7438X_{ts} + 9.4700X_{cum} \quad r^2 = 0.999994 \tag{1}$$

$$b[\text{Å}] = 18.0562X_{tr} + 17.936X_{ts} + 17.925X_{cum} \quad r^2 = 0.999997 \tag{2}$$

$$c[\text{Å}] = 5.2768X_{tr} + 5.2995X_{ts} + 5.2700X_{cum} \quad r^2 = 0.999999 \tag{3}$$

$$\beta[^\circ] = 104.74X_{tr} + 105.68X_{ts} + 102.18X_{cum} \quad r^2 = 0.999996 \tag{4}$$

The high correlation of the linear regressions ($r^2 > 0.999$) supports the assumption that the lattice parameters are, in fact, a linear function of the composition. Jenkins (1994) extrapolated a similar cell volume of 892.9 ± 1.2 $Å^3$ for the tschermakite end member. The results of the regression are also plotted in Fig. 5, which demonstrates that the lattice parameters a and β are also

sensitive to the cummingtonite content of the solid solution.

Because of their small grain size, compositions of synthetic tremolite–tschermakite solid solutions often have been determined by XRD using the location of the (310) reflection (Jenkins 1981, 1983, 1988; Cho and Ernst 1991; Hoschek 1995). The location of the (310) reflection calculated using Eqs. (1)–(4) for cummingtonite contents of 0 and 10 mol% and the calibration curves used by Jenkins (1988), Cho and Ernst (1991) and Hoschek (1995) are shown in Fig. 7. These calibration curves coincide with the calculated line for a cummingtonite content of 10 mol%. If these latter curves were used for amphiboles with lower cummingtonite contents, the tschermakite content would be severely underestimated. If the cummingtonite content is 0 instead of 10 mol%, the tschermakite content thus derived will be 18 mol% too low using the calibration curves previously available.

An alternate way of determining compositions by XRD is the use of the compositional dependence of the lattice parameters. The lattice parameters a and β are sensitive to both the tschermakite and cummingtonite content. While a decreases with increasing tschermakite and increasing cummingtonite content, β increases with increasing tschermakite content but decreases with increasing cummingtonite content. The combination of Eqs. (1) and (4) yields expressions for the composition of an amphibole sample, if its lattice parameters are known, on the tremolite–tschermakite–cummingtonite ternary:

$$X_{ts} = \frac{(a_{sample} - a_{cum})(\beta_{tr} - \beta_{cum}) - (a_{tr} - a_{cum})(\beta_{sample} - \beta_{cum})}{(a_{tr} - a_{cum})(\beta_{cum} - \beta_{ts}) - (a_{cum} - a_{ts})(\beta_{tr} - \beta_{cum})} \quad (5)$$

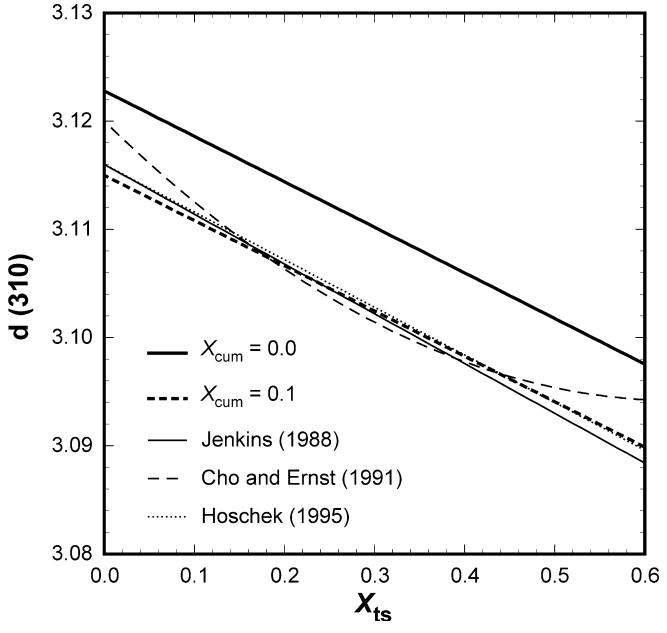

Fig. 7 Variation of the $d(310)$ reflection with composition of Al tremolites

$$X_{tr} = \frac{(a_{sample} - a_{cum})(\beta_{ts} - \beta_{cum}) - (a_{ts} - a_{cum})(\beta_{sample} - \beta_{cum})}{(a_{ts} - a_{cum})(\beta_{cum} - \beta_{tr}) - (a_{cum} - a_{tr})(\beta_{ts} - \beta_{cum})} \quad (6)$$

$$X_{cum} = \frac{(a_{sample} - a_{tr})(\beta_{tr} - \beta_{ts}) - (a_{tr} - a_{ts})(\beta_{sample} - \beta_{tr})}{(a_{tr} - a_{ts})(\beta_{ts} - \beta_{cum}) - (a_{ts} - a_{cum})(\beta_{tr} - \beta_{ts})}. \quad (7)$$

Oba (1978) presented lattice constants of several tschermakites which were synthesized between 800 and 850 °C and 700 and 1700 MPa. The composition of these tschermakites was evaluated using the a–β relationship of Eqs. (5)–(7). The derived tschermakite contents were between $X_{ts} = 0.36$ and 0.55. This is a strong indication that pure tschermakite was not synthesized in Oba's study.

IR

OH-stretching vibration and occupancy of sites

The frequency of the fundamental OH-stretching vibration is a function of the local charge distribution in the neighbourhood of the proton (Burns and Strens 1966; Hawthorne 1981). The cation sites in the vicinity of the proton are illustrated in Fig. 8. This figure shows the central layer of octahedral sites within the amphibole I beam, the tetrahedra belonging to the upper (Si, Al)$_4$O$_{11}$ chain, the M4 sites belonging to this I beam and the upper left and right neighbour I beams (M4*). The tetrahedra of the lower double chain are not shown because the effect of any variation in charge distribution in this chain which could influence the vibration of the upper proton is, as a first approximation, shielded by the octahedral chain. In the following, proton–cation distances up to 6 Å were considered, which are calculated using the structure of tremolite, as determined by

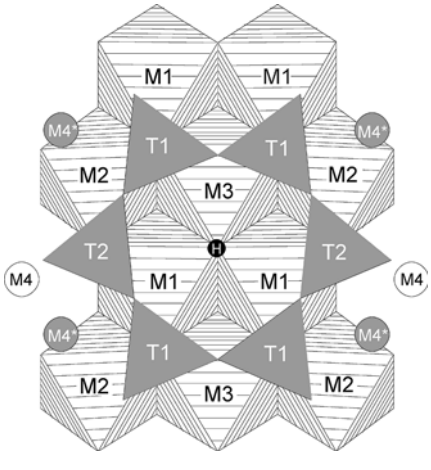

Fig. 8 Local environment of the proton in the tremolite structure. The M4 sites (*white*) are on a level with the octahedral strip. The M4* sites (*grey*) belong to adjacent upper left and right neighbour I beams

Hawthorne and Grundy (1976); (cf. Table 4). The distances range between 2.67 and 5.81 Å. It must be noted that several sites (e.g., M2, M3, M4) occur with different distances in the immediate vicinity of the proton.

In tremolite, cations in the immediate vicinity of the proton are Mg^{2+} on M1, M2 and M3, Ca^{2+} on M4 and Si^{4+} on T1 and T2 sites. The corresponding band is located at 3675 cm^{-1} (Burns and Strens 1966). If cations with other radii and charges are substituted on these sites, the band position for this local configuration will be different. In solid solutions, various configurations occur simultaneously and various bands are observed (e.g., Burns and Strens 1966; Della Ventura et al. 1999; Gottschalk et al. 1998, 1999; Hawthorne et al. 2000). The absorbance of such bands will be proportional to the probability of its corresponding configuration. If the absorbance of each band is evaluated, then the probability of each configuration and therefore the site occupancies can be determined. The problem is however, the effective size of the configuration shell, the assignment of a band to a certain configuration and the wavenumber dependency of the absorbency.

Band positions

A detailed inspection of the IR spectra in the range of the OH-stretching vibrations revealed that the observed bands, centred at 3675, 3652, 3624 and 3608 cm^{-1}, had shoulders and/or were asymmetric. By fitting the spectra to symmetric bands of a Gaussian-Lorentzian character, up to 12 individual bands could be identified, which are listed in Table 5. The identified bands had within each sample a variety of different FWHMs which increased with decreasing wavenumber and generally increased with increasing Al content. In addition, the absorbance of some bands increased with Al content while others decreased. According to their FWHMs, the bands were grouped into three band systems which were located between 3664 and 3676 cm^{-1} (I), 3633 and 3664 cm^{-1} (II) and 3526 and 3633 cm^{-1} (III). To simplify the process of the quantification and interpretation of the bands, the FWHMs within each band system were constrained to one single value. With this constrain it was possible to obtain consistent band positions also for the band systems with high FWHMs (II + III) along the whole solid-solution series. Band positions, relative integral absorbances and FWHMs of the detected bands are shown Table 5. The fitted bands for the runs TS-30, TS-64, TS-92 and TS-93 with different Al contents are shown in Fig. 9.

Table 4 Cation–proton distances of a tremolite *I* beam up to 6 Å. (Hawthorne and Grundy 1976)

Proton distance to	Near (Å)	Far (Å)
M1	2.692	5.105
M2	4.164	5.144
M3	2.670	4.032
M4	5.465	–
M4*	5.318	5.812
T1	3.120	3.126
T2	3.183	–

Local configurations

Previous studies concluded that Al^{3+} in octahedral coordination ($^{[6]}Al$) either predominantly occupies only the M2 (Hawthorne 1981, 1983), the M2 and M1/M3 (Raudsepp et al. 1987; Welch 1994) or the M2 and M3 sites (Oberti et al. 1995a; Welch and Knight 1999; Della Ventura et al. 1999; Hawthorne et al. 2000). Jenkins et al. (1997) concluded from their ^{29}Si NMR spectra that Al^{3+} is equally distributed between the T1 and T2 sites. According to Hawthorne (1981, 1983) and Welch et al. (1998), tetrahedral Al ($^{[4]}Al$) is preferentially incorporated at the T1 site. Oberti et al. (1995b) observed that high Al contents ($^{[4]}Al > 2$ apfu) and equilibration at high temperatures lead to increasing $^{[4]}Al$ occupancies at T2. For the following considerations it is assumed that in the tremolite–tschermakite solid solution $^{[6]}Al$ occupies either only the M2 or the M2 and M3 sites. The M1 site will always be filled by Mg^{2+}. Synthesis temperatures were below 850 °C and the maximum $^{[4]}Al$ contents was 1.04 apfu. Therefore, it has been assumed that $^{[4]}Al$ is preferentially located at the T1 site. For simplicity, the substitution of Mg^{2+} for Ca^{2+} on the M4 site (cummingtonite component) is neglected. The resulting relevant cluster is shown in Fig. 10 and contains four M2, two M3 and eight T1 sites, two protons, one above (H) and one below (H′) the octahedral strip. The tetrahedra above and below the octahedral chain will be further also labelled T1 and T1′, respectively. Because of the assumption that the octahedral chain acts as a shield, the vibrational mode of a proton is influenced only by the four T1 cations on the same level. The distances between the proton and the M2 and M3 sites in the front and in the back (according to Fig. 10) are different (Table 4) and therefore the $M2_{near}$, $M3_{near}$ and $M2_{far}$, $M3_{far}$ sites are treated separately. In the following as a shorthand notation, each configuration will be designated by M2M3M2:T1T1-T1T1:M2M3M2 which lists, according to Fig. 10, the front (far) sites first (all sites from left to right). In this notation the configuration typical for tremolite will MgMgMg:SiSi–SiSi:MgMgMg (configuration A1, see Fig. 11).

Due to local charge balance, the tschermakite exchange is supposed to be a coupled substitution. It is now reasonable to assume that the substitution of Al^{3+} for Mg^{2+} on either M2 or M3 is charge-balanced by Al^{3+} for Si^{4+} on the closest T1 site. If one Al^{3+} is substituted on the left front M2 site, the upper proton H will have either the configuration AlMgMg:AlSi–SiSi:MgMgMg (A4) or AlMgMg:SiSi–SiSi:MgMgMg (A2). For the second configuration the charge balance occurs on a T1′ site. The lower proton H′ will have one of the corresponding and matching configuration, either

Table 5 Data of the OH-stretching vibration of the synthesized Al tremolites. Position, relative absorbance, full width at half maximum (FWHM) of fitted bands. Runs are listed with increasing X_{ts}, derived from XRD data

	Run		TS-83	TS-33	TS-82	TS-15	TS-64	TS-86	TS-40	TS-6	TS-19	TS-30	TS-52	TS-92	TS-93
	X_{ts}		0.08	0.13	0.16	0.17	0.18	0.19	0.19	0.22	0.32	0.32	0.39	0.44	0.52
Band system I	Band A	(cm^{-1})	3674.7	3675.1	3674.9	3675.1	3675.0	3674.9	3675.3	3675.0	3675.0	3675.1	3674.9	3674.9	3675.4
	Rel. absorb.	(%)	58.2	50.9	35.6	38.5	46.8	31.9	45.0	26.9	17.0	17.0	9.8	6.3	2.7
	Band B	(cm^{-1})	3671.7	3672.1	3671.9	3672.1	3671.9	3671.7	3672.2	3671.9	3672.0	3671.9	3671.7	3672.4	3672.4
	Rel. absorb.	(%)	10.1	6.4	9.5	10.8	9.1	11.7	9.2	9.5	7.9	9.1	5.0	4.5	3.7
	Band C	(cm^{-1})	3669.1	3669.6	3669.4	3669.5	3669.5	3669.1	3669.5	3669.2	3669.2	3669.1	3669.3	3669.4	3669.5
	Rel. absorb.	(%)	10.6	4.9	9.4	7.2	7.4	9.0	6.4	6.7	6.7	7.6	4.3	6.5	3.1
	Band D	(cm^{-1})	3666.3	3667.4	3666.5	3666.5	3666.6	3665.9	3666.2	3666.1	3666.0	3665.8	3666.2	3665.5	3665.5
	Rel. absorb.	(%)	2.2	0.7	3.3	2.8	2.2	3.4	2.0	2.3	2.6	3.3	2.6	3.3	2.5
	FWHM A-D	(cm^{-1})	3.2	2.9	3.9	3.3	3.5	3.8	3.2	3.5	4.6	4.6	5.4	6.5	7.6
Band system II	Band E	(cm^{-1})	3660.7	3658.6	3661.4	3660.2	3659.7	3660.6	3660.7	3660.3	3660.2	3661.3	3660.9	3660.5	3660.3
	Rel. absorb.	(%)	3.4	7.0	8.1	6.3	4.2	6.9	4.6	9.5	11.3	11.4	12.6	12.8	9.0
	Band F	(cm^{-1})	3651.9	3651.3	3651.6	3650.9	3651.6	3651.1	3651.6	3651.7	3651.9	3651.0	3651.4	3651.9	3652.5
	Rel. absorb.	(%)	8.7	12.1	13.8	13.3	15.2	14.1	12.1	15.2	24.2	16.8	18.0	19.8	17.5
	Band G	(cm^{-1})	3641.1	3640.8	3640.5	3640.0	3640.7	3640.5	3640.6	3641.6	3641.6	3640.1	3641.3	3641.2	3641.9
	Rel. absorb.	(%)	2.8	4.9	5.5	5.6	4.9	6.4	5.0	8.3	8.6	7.3	7.4	9.0	9.5
	FWHM E-G	(cm^{-1})	10.2	11.4	11.9	10.9	11.0	11.3	10.2	12.3	15.0	13.0	15.7	16.0	16.9
Band system III	Band H	(cm^{-1})	3623.7	3623.7	3624.1	3624.2	3623.9	3624.5	3624.2	3624.5	3624.2	3624.8	3625.4	3625.1	3624.8
	Rel. absorb.	(%)	2.6	7.3	9.9	10.3	6.6	11.0	10.6	13.4	16.7	19.1	22.0	24.5	31.0
	Band I	(cm^{-1})	3607.2	3607.0	3608.4	3607.1	3608.3	3607.9	3607.0	3607.4	3608.0	3606.8	3607.9	3608.2	3607.0
	Rel. absorb.	(%)	1.3	5.0	4.8	5.3	3.7	5.6	5.2	6.8	5.1	8.5	9.0	8.7	10.5
	Band J	(cm^{-1})											3583.4	3578.3	3567.9
	Rel. absorb.	(%)											5.7	3.2	7.1
	Band K	(cm^{-1})											3555.4	3552.9	3526.3
	Rel. absorb.	(%)											3.4	1.4	3.4
	FWHM H-K	(cm^{-1})	7.2	10.9	15.2	15.4	12.8	15.8	14.5	19.4	26.9	25.7	34.5	35.8	42.5
Triple chain band		(cm^{-1})		3660.8						3660.8					
	Rel. absorb	(%)		0.8						1.4					
	FWHM	(cm^{-1})		2.8						3.8					

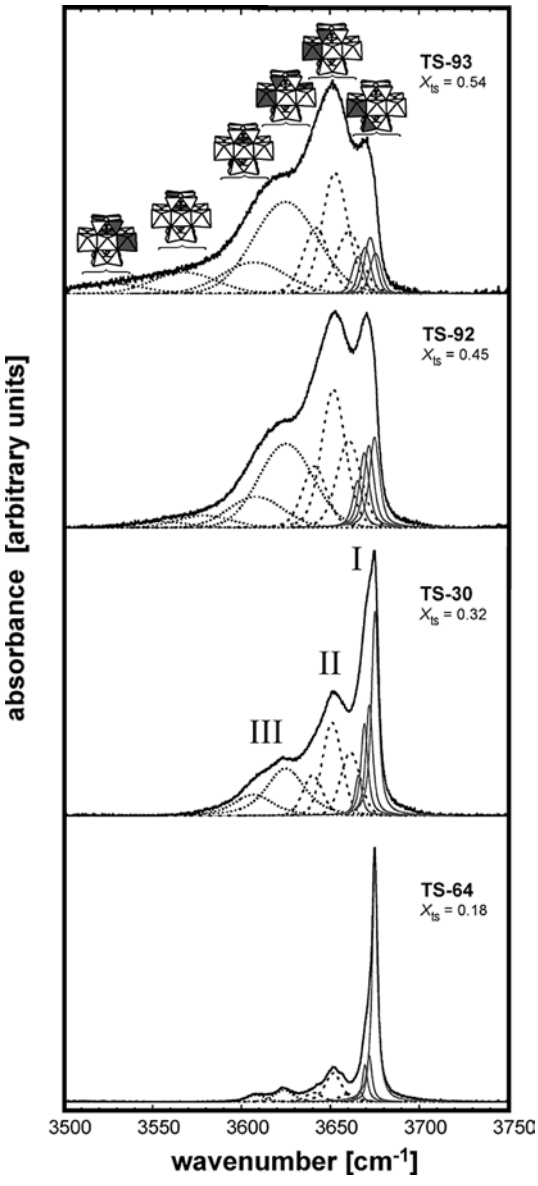

Fig. 9 Selected FTIR spectra of the runs TS-93, TS-92, TS-30 and TS-64. Up to 11 individual bands were necessary for a consistent fitting procedure along the whole solid-solution series. An exemplary band assignment to the configurations is shown. The tschermakite contents in amphibole (X_{ts}) were derived from XRD data

A2 or A4, respectively. The adjacent cluster to the front is formed in the *c* direction by the next two T1, two T1′, two M2 and one M3 sites. As a consequence, this cluster will then have the configuration either MgMgMg:SiSi–SiAl:AlMgMg (C1) or MgMgMg:SiSi–SiSi:AlMgMg (B1) if no additional Al^{3+} substitution occurs. If Al^{3+} is substituted on the front M3 site, the occurring configurations for H are either MgAlMg:AlSi–SiSi:MgMgMg (A6) or MgAlMg:SiSi–SiSi:MgMgMg (A3). In the more Al-rich amphiboles, it is possible that configurations with multiple substitutions will occur. Bond valence considerations (Oberti et al. 1995b; Hawthorne 1997) implied that ^{T1}Al–O–^{T1}Al dimers are very unlikely in amphiboles and that therefore Al avoidance operates.

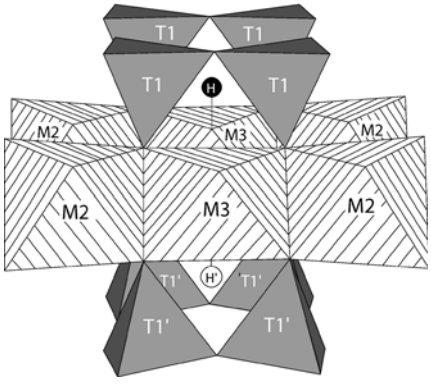

Fig. 10 Cluster around the H atom consisting only of polyhedra where Al substitution is assumed

Bond valence considerations also showed that cation arrangements with Al^{3+} on adjacent octahedral sites are improbable (Hawthorne 1997; Della Ventura et al. 1999; Hawthorne et al. 2000). These considerations lead to a total of 121 configurations. This number is reduced to 48 because some configurations are not distinguishable, e.g., the configuration MgAlMg:SiAl–SiSi:MgMgMg is equivalent to configuration MgAlMg:AlSi–SiSi:MgMgMg (A6), which therefore has a multiplicity of two. For each configuration there will be an OH-vibrational band with an absorbance proportional to its probability. If it is further assumed that the effect of substitution of two Al^{3+} at equivalent M2 or T1 sites either in *cis*- and *trans*-configuration is indistinguishable (e.g., AlMgMg:SiSi–SiSi:AlMgMg (B2) and AlMgMg:SiSi–SiSi:MgMgAl) the total number of different configurations is reduced to 36. These configurations with their multiplicities are summarized in Fig. 11.

It must be noted that the definition of the configuration shell for IR interpretation as in Fig. 10 comprises a larger size (and more cations) than in previous studies of synthetic Al tremolites. Jenkins et al. (1997) considered Al–Mg substitution at two M1 and one $M3_{near}$ sites in the nearest vicinity of the proton. Hawthorne et al. (2000) reported that the OH-stretching vibration of Al tremolites is also influenced by the next-nearest neighbours of the proton (T1T1 : M2M3M2). The interpretation model of the IR bands included Mg–Al substitution at $M2_{near}$, $M3_{near}$ and $M3_{far}$ sites and Si–Al substitution at T1 sites of the back of the cluster (Fig. 10). The front T1 and $M2_{far}$ sites were not included in the model by Hawthorne et al. (2000). It is known that even substitutions at M4 sites influence the fine structure of the OH band in tremolite (Gottschalk et al. 1998). Therefore, significant contributions to the absorbance can be expected by substitutions at T1 and $M2_{far}$ sites in the front of the cluster (Fig. 10), because these sites are at shorter distances to the proton than the M4 sites (Table 4). Furthermore, T1 sites at both the front and back of the cluster are at nearly the same distance to the proton (3.13 and 3.12 Å). Si–Al substitutions on the front T1 sites should have almost the same influence on

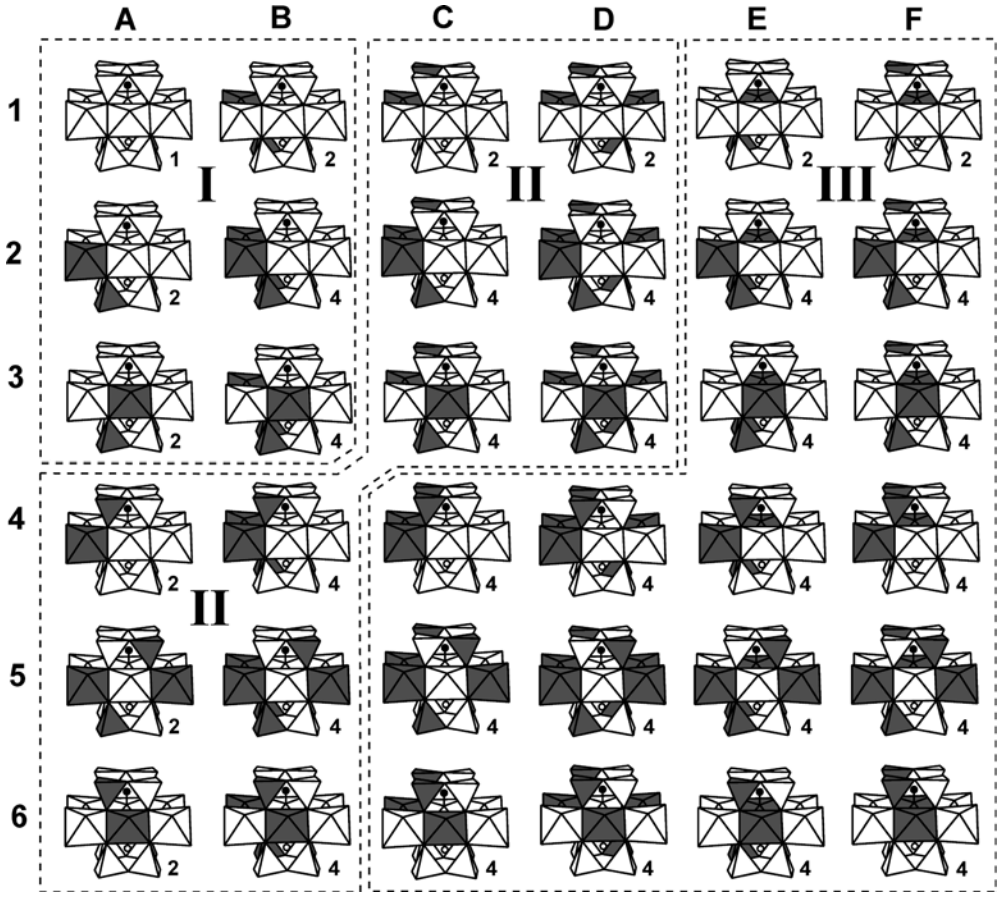

Fig. 11 The 36 possible configurations for Al incorporation assuming Al–Mg substitution at M2 and M3 sites and Al–Si substitution at T1 sites including charge-coupled substitution and Al avoidance. The *numbers* are the multiplicities of the configurations. *White tetrahedra* are occupied by Si and *white octahedra* are occupied by Mg. *Grey tetrahedra and octahedra* are occupied by Al

the OH-stretching vibration as substitutions on the back T1 sites. Thus, also configurations with two Si–Al substitutions on the four nearest T1 sites around a proton have to be considered. In Fig. 11 this comprises configurations C4-C6, D4-D6 and F4-F6 for the proton above and configurations B2-B3, B5, D2-D3, D5, E2-E3 and E5 for the proton below.

Band assignment

Up to 12 bands have been detected in the amphiboles synthesized here. This number is significantly lower than the expected 36. Many bands will overlap and are not resolved; others will be of low absorbance because of the low probability of their corresponding configuration. From these 12 detected bands only the one with the highest wavenumber at 3675 cm^{-1} is definitely known to correspond to the tremolite configuration (A1).

For synthetic tremolite–tschermakite solid solutions, Jenkins et al. (1997) observed with increasing Al content a decrease in the absorbance of the tremolite-type band at 3675 cm^{-1} and an increase in the band at 3652 cm^{-1}. The band at 3652 cm^{-1} was attributed to the Al^{3+} substitution on either the M1 or M3 site. Hawthorne et al. (2000) reported bands at 3675, 3671, 3655, 3642, 3624 and 3608 cm^{-1}. The model for band assignments based on four distinct substitutions: (1) Al ↔ Mg on $M3_{near}$, (2) Al ↔ Si on T1, (3) Al ↔ Mg on $M2_{near}$ and Al ↔ Mg on $M3_{far}$. The band at 3671 cm^{-1} was assigned to the substitution (3) and the band at 3655 cm^{-1} to the substitution (2). The band at 3642 cm^{-1} was attributed to either a combination of substitution (2) and (3) or only a substitution (1). Substitutions of either (1) and (3) or (1) and (2) caused the band at 3624 cm^{-1}. The band at 3608 cm^{-1} was assigned to combinations of substitution (1), (2) and (3). In this study a larger fine structure of the bands were observed. Band shoulders and asymmetries could not be explained with the model from Hawthorne et al. (2000). A consistent band fitting along the whole solid-solution series required a more expanded model, which included also Al substitutions on T1 and $M2_{far}$ sites at the front of the cluster (Fig. 10).

The physical environmental differences between the 36 configurations are due to differences in cation charge and cation radii of Al^{3+} (0.39 Å) vs. Si^{4+} (0.26 Å) in tetrahedral coordination and of Al^{3+} (0.54 Å) vs. Mg^{2+} (0.72 Å) in octahedral coordination, respectively (Shannon 1976). The influence of differences in both charge and size on the electrostatic field is complex and not easily predicted. Furthermore, the substitutions of a larger cation with a lower charge (tetrahedral) and of a smaller cation with a higher charge (octahedral), but at the opposite site of the proton, both yield bands at lower wavenumbers. For purposes of simplification, it is assumed that the shift of the band position with respect to

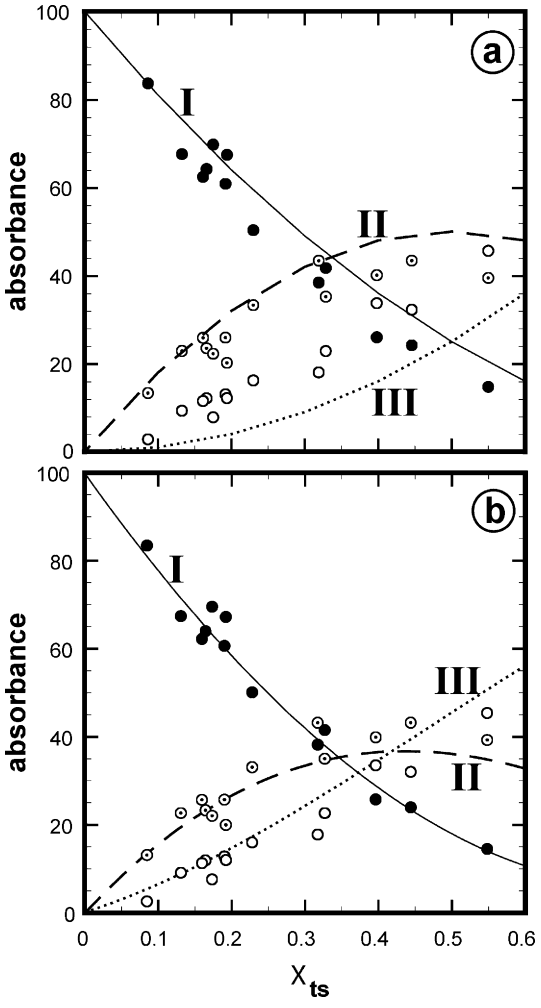

Fig. 12a, b Comparison of observed (*points*) and calculated (*lines*) absorbances for each group (*I–III*). **a** Random distribution of Al–Mg on the M2 sites. **b** Random distribution of Al–Mg on the M2 and M3 sites. *Filled circles* band group I; *open circles with dots* band group II; *open circles* band group III

the tremolite band is correlated with the distance at which Al^{3+} substitution occurs. The distances of the M2, M3 and T1 sites to the proton (Table 4) can also be divided into three groups. One of the two M3 sites is closest to the proton (2.67 Å). This is followed by the four T1 sites (3.12 and 3.13 Å). The two M2 sites (far and near) and the other $M3_{far}$ site show the largest distances (4.16, 5.14 and 4.03 Å, respectively). Therefore, an Al^{3+} substitution on the most remote sites should have the least influence on band position. The influence of Al^{3+} on T1 sites would be larger, followed by Al^{3+} substitution on the $M3_{near}$ site with the largest influence on band position. Similarly, the effect of the two Al^{3+} substitutions should be a linear combination. According to these assumptions, the configurations can be assigned to three groups. I: only Si^{4+} at T1 and one to two Al^{3+} on M2 and/or $M3_{far}$, II: one Al^{3+} on T1 and one to three Al^{3+} on M2 and/or on the $M3_{far}$, III: either Al^{3+} on $M3_{near}$ and/or two Al^{3+} on T1 and an additional one to four Al^{3+} on M2.

It is now assumed that the three configurational groups (I–III) correspond to the three groups of bands with fundamental differing FWHMs (Table 5).

The six configurations of the group I (A1 to A3 and B1 to B3) are assigned to the band A, B, C and D. The bands B, C and D closest to the tremolite band A were all characterized by a low FWHM (Table 5). If only octahedral substitutions are relevant for a configuration, such low FWHMs are commonly observed (e.g., Gottschalk et al. 1998, 1999). Therefore, it seems reasonable to assign these bands to the group I. The shift of positions for bands B, C and D with respect to band A was in the range of −3 to −10 cm^{-1}. With increasing Al content, the absorbance of A decreased and that of B, C and D increased. The D band always showed the lowest absorbance of these. Because the total X_{ts} of the synthesized amphiboles does not exceed 0.54, the probability of corresponding configurations with two Al^{3+} substitutions in one cluster is lower than those of the other four. Therefore, one might speculate that the B and D bands correspond to the configurations B2 and B3. As a consequence of the distance argument, the B band would correspond to the A2 configuration, the C band to A3 + B1 and the D band to B2 + B3 configurations.

There are 12 configurations with one Al^{3+} on T1 and one Al^{3+} on M2 and $M3_{far}$. These resulting bands are assumed to be those of the group II. The shift in the position of bands E, F and G with respect to band A was in the range of −15, −24 and −34 cm^{-1}, respectively.

The remaining configurations have either Al^{3+} on $M3_{near}$ and/or two Al^{3+} on T1. The corresponding bands are considered to be those of group III. The position of bands H, I, J and K showed a shift of −51, −68, ∼−90 and ∼−120 cm^{-1}, respectively.

An exact assignment of the bands in the groups II and III to distinct configurations is difficult. One could, however, speculate that the shift of the H band (−51 cm^{-1}) is due to two Al^{3+} substitutions on T1 because the average shift of the group-II bands (one Al^{3+} on T1) is −24 cm^{-1}. The I band (−68 cm^{-1}) could then be assigned to a single substitution on $M3_{near}$. Consequently, the J band could be due to an $M3_{near}$ and one T1 (∼−90 cm^{-1}) and the K band to an $M3_{near}$ and two T1 (∼−120 cm^{-1}) substitutions. This band assignment is shown in Fig. 9.

An additional small sharp band of low absorbance was observed in the samples TS-6 and TS-33 at 3660.8 cm^{-1}, which is not consistent with the band systems described above. Gottschalk et al. (1998, 1999) reported minor bands in synthetic tremolites at 3660 cm^{-1} which correlated with the concentrations of chain multiplicity faults. This is in agreement with the results of HRTEM investigations for TS-33, which showed a high concentration of chain multiplicity faults.

Quantification of site occupancies

Hawthorne et al. (2000) discussed that it is not possible to quantify the OH bands of synthetic Al tremolites

because no satisfactory background could be fitted. Powder IR samples of amphiboles were usually prepared from a mixture of the amphibole sample and KBr. KBr contains small amounts of water under normal conditions. IR spectra of water-bearing KBr show very broad absorbance bands which overlap with the region of the OH-stretching vibration of amphiboles. The overlapping broad water band makes a quantitative evaluation of the OH band rather difficult. Good results can be obtained, however, if the KBr powder and the prepared KBr pellets are dried at 170 °C for at least 48 h, but typically for several weeks, to minimize water contamination in the samples. After such a procedure, the IR spectra showed a flat baseline. In most cases, the background could be subtracted using a linear function and only in some rare cases using a cubic function. Using these samples a quantitative interpretation of the IR spectra was possible.

As described above, the observed three band systems in Al tremolites are assigned to three configurational groups. The absorbance of each band should be proportional to the probability of its underlying configuration. The observed absorbances should therefore provide some information about the actual site occupancies. To do this, the functional dependence of absorptivity with respect to wavenumber is required.

The absorptivity of the OH-stretching vibration is a linear function of wavenumber (Skogby and Rossmann 1991). Hawthorne et al. (1997) determined and Melzer et al. (2000) further quantified the required proportionality factor using synthetic K–richterite–tremolite and K–richterite–richterite-tremolite solid solutions, respectively. Melzer et al. (2000) derived the following expression for the absorptivity of an OH-stretching band at the wavenumber w relative to the tremolite band at 3674.6 cm^{-1}:

$$\varepsilon_w/\varepsilon_{3674.6}\,cm^{-1} = 1 - 0.00703(w - 3674.6) \quad . \qquad (8)$$

This expression was derived in the range of 3674–3730 cm^{-1} and for the synthetic Al amphiboles it had to be extrapolated to lower wavenumbers. All absorbances were corrected using Eq. (8). The corrected absorbances should be directly proportional to the probabilities of a single configuration or group of configurations.

The probability of possible configurations were simulated with a Monte-Carlo approach. Using a model crystal containing 3000 tremolite configurations of the type A1, a chosen number of Al^{3+} cations corresponding to a desired X_{ts} content were randomly distributed. Two models were set up: (1) Al^{3+} substitution only on M2 and T1 and (2) Al^{3+} substitution on M2, M3 and T1 with no next-neighbour $^{[6]}Al$. The constraints of local charge balance ($^{[6]}Al$–O–$^{[4]}Al$ coupling) and Al avoidance (no $^{[4]}Al$–O–$^{[4]}Al$) were applied. At the end of each simulation, the probabilities of all configurations were determined. Identical configurations from the proton above and the proton below were summed up.

The simulation was carried out for seven different tschermakite contents between $X_{ts} = 0.0$ and 0.6 using step intervals of 0.1. The results are presented in Fig. 12, which shows the sum of probabilities vs. the corrected absorbances within each group (I–III) of configurations. Figure 12a shows that the assignment of bands to certain groups of configurations is correct. Furthermore, the second model in Fig. 12b (Al^{3+} on M2 and M3) seems to be more appropriate. This indicates that octahedral substitution of Al^{3+} is not restricted only to the M2 site in Al tremolites. This is in agreement with NMR and IR investigations of synthetic Al tremolites (Jenkins et al. 1997; Hawthorne et al. 2000). It supports the results of single-crystal X-ray studies of pargasites and pargasitic hornblendes (Oberti et al. 1995a) and a neutron powder diffraction study of synthetic pargasite (Welch and Knight 1999) where Al is distributed over M2 and M3 sites.

The relative intensity of band system III is significantly increased with rising Al content in tremolite. For magnesiohornblende a proportion of 50% of band system III is attributed to configurations with two Al on the nearest T1 sites around a proton (Fig. 11, e.g., for proton above: configurations C4-C6, D4-D6 and F4-F6). Such (SiAl)(SiAl) configurations correspond to $Q^2(2Al)$ configurations in ^{29}Si MAS NMR spectra. Interestingly, low $Q^2(2Al)$ proportions in ^{29}Si MAS NMR studies indicated a very low Al clustering in the tetrahedral chain of amphiboles (Welch et al. 1998). However, it can be shown that the relative proportions of $Q^2(2Al)$ and (SiAl)(SiAl) configurations are not directly comparable. First, Al incorporation on T1 sites in amphiboles creates a higher number of NMR configurations [$Q^2(0Al)$, $Q^2(1Al)$, $Q^2(2Al)$, $Q^3(0Al)$ and $Q^3(1Al)$] compared to IR configurations [(SiSi)(SiSi), (SiSi)(SiAl) and (SiAl)(SiAl)]. It lowers the relative proportion of $Q^2(2Al)$ compared to (SiAl)(SiAl). Second, $Q^2(2Al)$ represents only (SiAl)(SiAl) *meta* configurations (see Welch et al. 1998). (SiAl)(AlSi) *para* configurations are part of $Q^2(1Al)$, which also lower the relative proportion of $Q^2(2Al)$. Summarizing, we believe that configurations of two Al on the nearest T1 sites around a proton in amphiboles cannot be neglected. The IR technique is a very useful method to detect such configurations.

Acknowledgments J.N. gratefully acknowledges the financial and technical support of the GeoForschungsZentrum Potsdam. The authors acknowledge the support and contributions of W. Heinrich. We thank R. Wirth for assistance with the TEM, O. Appelt and D. Rhede for assistance with the EMP, as well as U. Glenz for assistance with the SEM. We also thank I. Bauer, E. Schemmert, K. Paech for their help in sample preparation and R. Schulz for technical help at the piston-cylinder and hydrothermal apparatus. Reviews by D. Harlov, A. Feenstra and M. Andrut improved earlier versions of this paper.

References

Burns RG, Strens RGJ (1966) Infrared study of the hydroxyl bands in clinoamphiboles. Science 153: 890–892

Cao RL, Ross C, Ernst WG (1986) Experimental studies to 10 kb of the bulk composition $tremolite_{50}$–$tschermakite_{50}$ + excess H_2O. Contrib Mineral Petrol 93: 160–167

Cho M, Ernst WG (1991) An experimental determination of calcic amphibole solid solution along the join tremolite–tschermakite. Am Mineral 76: 985–1001

Della Ventura G, Robert J-L, Raudsepp M, Hawthorne FC (1993) Site occupancies in monoclinic amphiboles: Rietveld structure refinement of synthetic nickel–magnesium–cobalt–potassium–richterite. Am Miner 78: 633–640

Della Ventura G, Hawthorne F, Robert J-L, Delbove F, Welch M, Raudsepp M (1999) Short-range order of cations in synthetic amphiboles along the richterite–pargasite join. Eur J Mineral 11: 79–94

Gottschalk M, Andrut M (1998) Structural and chemical characterization of synthetic (Na,K)-richterite solid solutions by EMP, HRTEM, XRD and FTIR spectroscopy. Phys Chem Miner 25: 173–480

Gottschalk M, Najorka J, Andrut M (1998) Structural and compositional characterisation of synthetic (Ca,Sr)-tremolite and (Ca,Sr)-diopside solid solutions. Phys Chem Miner 25: 415–428.

Gottschalk M, Andrut M, Melzer S (1999) The determination of cummingtonite content of synthetic tremolite. Eur J Mineral 11: 967–982.

Graham CM, Maresch WV, Welch MD, Pawley AR (1989) Experimental studies on amphiboles: a review with thermodynamic perspectives. Eur J Mineral 1: 535–555

Hawthorne FC (1981) Crystal chemistry of the amphiboles. In: Veblen DR (ed) Amphiboles and other hydrous pyriboles—mineralogy. Reviews in mineralogy, vol 9A. Mineral Society of America, Washington, DC, pp 1–102.

Hawthorne FC (1983) The crystal chemistry of the amphiboles. Can Mineral 21: 173–480

Hawthorne FC (1997) Short-range order in amphiboles: a bond–valence approach. Can Mineral 35: 201–216

Hawthorne FC, Grundy HD (1976) The crystal chemistry of amphiboles. IV. X-ray and neutron refinements of the crystal structure of tremolite. Can Mineral 14: 334–345

Hawthorne FC, Della Ventura G, Robert J-L, Welch MD, Raudsepp M, Jenkins DM (1997) A Rietveld and infrared study of synthetic amphiboles along the potassium–richterite–tremolite join. Am Mineral 82: 708–716

Hawthorne FC, Welch MD, Della Ventura G, Liu S, Robert J-L, Jenkins DM (2000) Short-range order in synthetic aluminous tremolites: an infrared and triple-quantum MAS NMR study. Am Mineral 85: 1716–1724

Hirschmann M, Evans BW, Yang H (1994) Composition and temperature dependence of Fe–Mg ordering in cummingtonite–grunerite as determined by X-ray diffraction. Am Mineral 79: 862–877

Hoschek G (1995) Stability relations and Al content of tremolite and talc in CMASH assemblages with kyanite + zoisite + quartz + H_2O. Eur J Mineral 7: 353–362

Jasmund K, Schäfer R (1972) Experimentelle Bestimmung der *P*–*T*-Stabilitätsbereiche in der Mischkristallreihe Tremolit–Tschermakit. Contrib Mineral Petrol 34: 101–115

Jenkins DM (1981) Experimental phase relations of hydrous peridotites modelled in the system H_2O–CaO–MgO–Al_2O_3–SiO_2. Contrib Mineral Petrol 77: 166–176

Jenkins DM (1983) Stability and composition relations of calcic amphiboles in ultramafic rocks. Contrib Mineral Petrol 83: 375–384

Jenkins DM (1987) Synthesis and characterization of tremolite in the system H_2O–CaO–MgO–SiO_2. Am Mineral 72: 707–715

Jenkins DM (1988) Experimental study of the join tremolite-tschermakite: a reinvestigation. Contrib Mineral Petrol 99: 392–400

Jenkins DM (1994) Experimental reversal of the aluminium content in tremolitic amphiboles in the system H_2O–CaO–MgO–Al_2O_3–SiO_2. Am J Sci 294: 593–620

Jenkins DM, Sherriff BL, Cramer J, Xu Z (1997) Al, Si, and Mg occupancies in tetrahedrally and octahedrally coordinated sites in synthetic aluminous tremolite. Am Mineral 82: 280–290

Larson AC, Von Dreele RB (1987) Generalized structure analysis system. Los Alamos National Laboratory Report

Manning GE (1994) The solubility of quartz in H_2O in the lower crust and upper mantle. Geochim Cosmochim Acta 58: 4831–4839

Melzer S, Gottschalk M, Heinrich W (1998) Experimentally determined partitioning of Rb between richterites and aqueuos (Na,K)-chloride solutions. Contrib Mineral Petrol 133: 315–328

Melzer S, Gottschalk M, Andrut M, Heinrich W (2000) Crystal chemistry of K—richterite–richterite–tremolite solid solutions: a SEM, EMP, XRD, HRTEM and IR study. Eur J Mineral 12: 273–291

Oba T (1978) Phase relations of $Ca_2Mg_3Al_2[Al_2Si_6O_{22}/(OH)_2]$–$Ca_2Mg_5[Si_8O_{22}/(OH)_2]$ join at high temperature and pressure – the stability of tschermakite. J Fac Sci Hokkaido Univ, ser. IV, 18: 339–50

Oberti R, Hawthorne FC, Ungaretti L, Cannillo E (1995a) $^{[6]}$Al disorder in amphiboles from mantle peridotites. Can Mineral 33: 867–878

Oberti R, Ungaretti L, Cannillo E, Hawthorne FC, Memmi I (1995b) Temperature-dependent Al order–disorder in the tetrahedral double chain of *C*2/*m* amphiboles. Eur J Mineral 7: 1049–1063

Pawley AR, Graham CM, Navrotsky A (1993) Tremolite–richterite amphiboles: synthesis, compositional and structural characterization, and thermochemistry. Am Mineral 78: 23–35

Pouchou JL, Pichoir F (1984) Un nouveau modèle de calcul pour la microanalyse quantitative par spectrométrie de rayons X. Rech Aérosp 3: 167–192

Quirion DM, Jenkins DM (1998) Dehydration and partial melting of tremolitic amphibole coexisting with zoisite, quartz, anorthite, diopside, and water in the system H_2O–CaO–MgO–Al_2O_3–SiO_2. Contrib Mineral Petrol 130: 379–389

Raudsepp M, Turnock AC, Hawthorne FC, Sherriff BL, Hartman JS (1987) Characterization of synthetic pargasitic amphiboles ($NaCa_2Mg_4M^{3+}Si_6\ Al_2O_{22}(OH,F)_2$; M^{3+} = Al, Cr, Ga, Sc, In) by infrared spectroscopy, Rietveld structure refinement, and ^{27}Al, ^{29}Si, and ^{19}F MAS NMR spectroscopy. Am Mineral 72: 580–593

Shannon RD (1976) Revised effective ionic radii and systematic studies of interatomic distances in halides and chalcogenides. Acta Crystallogr (A)32: 751–767

Skogby H, Rossmann GR (1991) The intensity of amphibole OH bands in the infrared absorption spectrum. Phys Chem Miner 18: 64–68

Smelik EA, Jenkins DM, Navrotsky A (1994) A calorimetric study of synthetic amphiboles along the tremolite–tschermakite join and the heats of formation of magnesiohornblende and tschermakite. Am Mineral 79: 1110–1122

Welch MD (1994) A multinuclear study of synthetic pargasite. Am Mineral 79: 261–268

Welch MD, Knight KS (1999) A neutron powder diffraction study of cation ordering in high-temperature synthetic amphiboles. Eur J Mineral 11: 321–331

Welch MD, Shuangxi L, Klinowski J (1998) ^{29}Si MAS NMR systematics of calcic and sodic-calcic amphiboles. Am Mineral 83: 85–96

Zimmermann R, Heinrich W, Franz G (1996) Tremolite synthesis from $CaCl_2$-bearing aqueous solutions. Eur J Mineral 8: 767–776